Received: 12 November 2024 | Revised: 7 February 2025 | Accepted: 11 February 2025

DOI: 10.1002/alz.70087

Alzheimer's & Dementia®
THE JOURNAL OF THE ALZHEIMER'S ASSOCIATION

RESEARCH ARTICLE

Pathways underlying selective neuronal vulnerability in Alzheimer's disease: Contrasting the vulnerable locus coeruleus to the resilient substantia nigra

Alexander J. Ehrenberg[1,2,3,4] | **Cathrine Sant**[5,6] | **Felipe L. Pereira**[1] | **Song Hua Li**[1] | **Jessica Buxton**[4] | **Sonali Langlois**[2] | **Marena Trinidad**[3] | **Ian Oh**[1] | **Renata Elaine Paraizo Leite**[7] | **Roberta Diehl Rodriguez**[7] | **Vitor Ribeiro Paes**[7] | **Carlos Agusto Pasqualucci**[7] | **William W. Seeley**[1] | **Salvatore Spina**[1] | **Claudia K. Suemoto**[8] | **Sally Temple**[9] | **Daniela Kaufer**[2,4] | **Lea T. Grinberg**[1,7,10]

[1]Memory and Aging Center, Weill Institute for Neurosciences, University of California, San Francisco, California, USA

[2]Helen Wills Neuroscience Institute, Dept. of Neuroscience, University of California, Berkeley, California, USA

[3]Innovative Genomics Institute, University of California, Berkeley, California, USA

[4]Dept. of Integrative Biology, University of California, Berkeley, California, USA

[5]Gladstone Institute for Neurological Diseases, Gladstone Institutes, San Francisco, California, USA

[6]Neuroscience Graduate Program, University of California, San Francisco, California, USA

[7]Dept. of Pathology, University of São Paulo Medical School, São Paulo, Brazil

[8]Division of Geriatrics, University of São Paulo Medical School, São Paulo, Brazil

[9]Neural Stem Cell Institute, Rensselaer, New York, USA

[10]Global Brain Health Institute, University of California, San Francisco, California, USA

Correspondence
Lea T. Grinberg, Memory and Aging Center, Weill Institute for Neurosciences, University of California, 675 Nelson Rising Lane, Box 1207, Suite 190, San Francisco, CA 94158, USA.
Email: lea.grinberg@ucsf.edu

Funding information
Rainwater Charitable Foundation; National Institutes of Health, Grant/Award Numbers: P30 AG062422, T32 GM139780, K24AG053435, R01AG064314, R01AG060477, R01AG075802; UC Berkeley Greater Good Science Center; Fundacao de Apoio a Pesquisa do Estado de São Paulo, Grant/Award Numbers: 06/55318, 2009/09134-4, 2012/07526-5; Alzheimer's Association, Grant/Award Number: AARG-20-678884; UC Berkeley Neuro-AI Resilience Center

Abstract

INTRODUCTION: Alzheimer's disease (AD) selectively affects certain brain regions, yet the mechanisms of selective vulnerability remain poorly understood. The neuromodulatory subcortical system, which includes nuclei exhibiting a range of vulnerability and resilience to AD-type degeneration, presents a framework for uncovering these mechanisms.

METHODS: We leveraged transcriptomics and immunohistochemistry in paired samples from human *post mortem* tissue representing a vulnerable and resilient region—the locus coeruleus (LC) and substantia nigra (SN). These regions have comparable anatomical features but distinct vulnerability to AD.

RESULTS: We identified significant differences in cholesterol homeostasis, antioxidant pathways, KRAS signaling, and estrogen signaling at a bulk transcriptomic level. Notably, evidence of sigma-2 receptor upregulation was detected in the LC.

DISCUSSION: Our findings highlight pathways differentiating the LC and SN, potentially explaining the LC's selective vulnerability in AD. Such pathways offer potential targets of disease-modifying therapies for AD.

KEYWORDS
Alzheimer's disease, autopsy, catecholamines, dopamine, human, locus coeruleus, neuropathology, noradrenaline, substantia nigra, tauopathy, transcriptomics

Highlights

- Intraindividual comparative RNAseq was used to study selective vulnerability.
- Metallothionein genes are significantly enriched in the substantia nigra.
- Cholesterol homeostatic genes are significantly enriched in the locus coeruleus.
- The locus coeruleus is likely more susceptible to toxic amyloid beta oligomers.

1 | BACKGROUND

Alzheimer's disease (AD) is defined by the progression of amyloid beta (Aβ) plaques and tau-positive neurofibrillary tangles, closely linked to neuronal loss. A major challenge in understanding AD is uncovering pathways driving selective neuronal vulnerability, where specific neurons are disproportionately affected while others are spared. Research in this area has historically been constrained by classical neuropathological methods, which rely on cross-sectional data and often lack early-stage cases. At AD's end stage, determining whether observed molecular signatures are inherent vulnerability factors, secondary responses, compensatory mechanisms, or reflect spared cells becomes highly challenging. Moreover, inter-individual variability introduces significant heterogeneity into study cohorts, an issue amplified by modern "-omics" techniques.

Recent technological advancements and the growing availability of well-characterized early-stage AD cases have enabled detailed investigations into the molecular mechanisms of selective vulnerability. We devised a strategy to compare early-affected regions with cytoarchitecturally similar but disease-resistant regions in human *post mortem* tissue, aiming to uncover factors driving selective vulnerability in AD.

The neuromodulatory subcortical structures are among the first brain regions to accumulate AD-related tau inclusions and exhibit neuronal loss. Beyond the cholinergic basal forebrain, AD tau lesions have been over a dozen in > 12 subcortical nuclei even before the transentorhinal cortex is affected (i.e., Braak stage I), including the locus coeruleus (LC).[1–4]

The LC is the primary noradrenergic nucleus in the central nervous system, existing as two columns flanking the fourth ventricle in the dorsal pons, with widespread projections throughout the brain. Evolving ≈ 420 million years ago, the LC plays a crucial role in regulating various human behaviors, including arousal and hedonic tone. Even before Braak stage I in the AD pathological process, the LC shows a significant burden of AD tau inclusions, which intensify as the disease progresses.[5–8] Notably, between Braak stages 0 and I, there is already an observable decrease in the volume of the LC, with further reductions in estimated neuron populations starting at Braak stage III.[9] These early degenerative changes in the LC are believed to contribute to the neuropsychiatric symptoms often seen in AD before cognitive decline becomes apparent.[10–12] Altogether, these observations position the LC as a promising region for investigating factors linked to early neuronal vulnerability to AD.[13,14]

Cytoarchitectonically, the LC shares many similarities with another deeply conserved nucleus, the substantia nigra (SN). They both belong to the isodendritic core and the ascending reticular activating system, meaning they host large neurons with long and poorly myelinated neurons.[15,16] They also feature a conspicuous cytoplasmic pigment, neuromelanin, and feature tau neuronal cytoplasmic inclusions from Braak stage 0[2], and degenerate significantly in Lewy body disease (LBD). Still, the SN remains mostly resistant to AD-type neurodegeneration (i.e., neuronal loss) until late disease stages.[2,17] The underlying reasons for this pattern of differential vulnerability remain unclear. One possibility involves factors related to the physiological specialization of the two nuclei. For instance, the LC projects widely throughout the neocortex to regions with high metabolic demand, while the SN, comparatively, projects less diffusely. The high demand placed on the LC by its vast projections has been suggested to drive its selective vulnerability, but the exact mechanisms are unclear. Regardless, comparing the LC and SN offers a compelling approach to investigate the mechanisms driving selective vulnerability in humans.

The distinct susceptibility between the LC and SN in AD offers unique opportunities to explore the mechanisms underlying selective vulnerability. In this study, we compared gene expression in paired LC and SN samples from individuals at early stages of the AD pathological process aiming to uncover the molecular determinants driving these differential susceptibilities.

2 | METHODS

2.1 | Participant selection and neuropathologic assessment

Cases were sourced from the Biobank for Aging Studies at the University of São Paulo[18] and the Neurodegenerative Disease Brain Bank at

the University of California, San Francisco Memory and Aging Center, which is an Alzheimer's Disease Research Center.[19] Consent for brain donation was obtained from subjects or next of kin following the site-specific protocol approved by the relevant institutional review board and the study was performed in accordance with the ethical standards as laid down in the 1964 Declaration of Helsinki. In both brain banks, brain tissue was sampled for neuropathological diagnosis following National Alzheimer's Coordinating Center guidelines. Basic histological and immunohistochemical stains were made with the antibodies for phospho-Ser202 Tau (1:250, CP13, courtesy of P. Davies), TDP-43 (1:2000, 10782-2-AP, Proteintech), β-amyloid (1:500, MAB5206, Millipore), α-Synuclein (1:5000, LB509, courtesy of J. Trojanowsky and V. Lee). Final neuropathologic diagnosis was made by following current guidelines.[20–23]

For this study, we included cases with Braak stages 0 through III that had available frozen LC and SN tissue (Table 1, Data S1 in supporting information). We excluded cases with Lewy body inclusions, TAR DNA-binding protein 43 proteinopathy, a primary or contributing diagnosis of chronic traumatic encephalopathy, a primary or contributing diagnosis of a primary tauopathy, an Axis I psychiatric disorder, a *post mortem* interval > 24 hours, or gross non-neurodegenerative structural neuropathology. Initial case selection sought equal proportions of males and females and informant-reported race within Braak stages, as well as a similar age distribution between Braak stages.

TABLE 1 Demographics and case characteristics stratified by Braak stage for transcriptomic dataset.

	Case characteristics
Braak 0	*n* = 6, 33% female Mean age, 48y (range: 37–62) CDR-SOB > 0: 0 (0%) CERAD Absent: 6 (100%) Thal phase 0: 6 (100%)
Braak I	*n* = 4, 50% female Mean age, 54y (range: 46–61) CDR-SOB > 0: 0 (0%) CERAD Absent: 2 (50%) Thal phase 0: 2 (50%)
Braak II	*n* = 4, 25% female Mean age, 73y (range: 67–91) CDR-SOB > 0: 0 (0%) CERAD Absent: 1 (25%) Thal phase 0: 0 (0%)
Braak III	*n* = 8, 38% female Mean age, 79y (range: 72–90) CDR-SOB > 0: 1 (13%) CERAD Absent: 4 (50%) Thal phase 0: 3 (38%)
All cases	*n* = 22, 36% female Mean age, 65y (range: 37–91) CDR-SOB > 0: 1 (5%) CERAD Absent: 13 (59%) Thal phase 0: 11 (50%) Race: White (5, 23%), Brown (6, 27%), Black (9, 41%), Asian (1, 5%), Unk (1, 5%)

Note: Race data were reported by an informant originally in Portuguese. The English translation displayed here corresponds to: Branca, White; Negra, Black; Parda, Brown; Amarela, Asian.

Abbreviations: CDR-SOB, Clinical Dementia Rating Sum of Boxes; CERAD, Consortium to Establish a Registry for Alzheimer's.

RESEARCH IN CONTEXT

1. **Systematic review**: The authors reviewed the literature using traditional sources and preprint servers (e.g., PubMed, BioRxiv). While there are many papers studying transcriptomics in Alzheimer's disease *post mortem* tissue, fewer focus on subcortical neuromodulatory structures. Relevant references are appropriately cited.
2. **Interpretation**: Our findings suggest that the selective vulnerability of the locus coeruleus compared to the substanita nigra is due to differences in cholesterol homeostasis mechanisms, making the locus coeruleus more susceptible to toxic amyloid beta oligomers, and metallothionein protein expression, making the locus coeruleus more susceptible to heavy metal accumulation.
3. **Future directions**: The findings here propose pathways underlying the augmented vulnerability of the locus coeruleus to Alzheimer's disease relative to the substantia nigra. These proposed pathways should be adjudicated in models of subcortical neuromodulatory structures and, if verified, exploited as potential therapeutic targets.

2.2 | Sample collection and processing

The frozen half of the brainstem for selected cases was kept on dry ice during the dissection. A scalpel was used to shave down the midbrain until the pigmented SN was exposed. An additional 3 to 5 mm of midbrain was shaved down around the rostral portion of the SN, with borders defined by the pigmented area. The protruding portion of the SN was sliced off of the shaved-down face of the midbrain and put into RNAlater (AM7020, Invitrogen) to protect RNA in case of thawing during transport for processing. The sample in RNAlater was frozen down at −80°C and transported on dry ice (Figure S1 in supporting information).

The LC was isolated by excising a tissue block approximately 5 to 10 mm in length along the rostrocaudal axis and approximately 10 mm in depth from the fourth ventricle near the medial eminence. After removal, the pigmented area of the LC was identified. Tissue outside the pigmented LC border was then discarded. The isolated LC tissue was subsequently preserved in RNAlater and frozen.

Tissue homogenization and cell lysis were performed in TRIzol. After cell lysis, impurities were removed, and RNAse inhibition, total

RNA was extracted using phase separation. RNA quality and concentration were assessed using an Agilent Bioanalyzer 2100. Samples with an RNA integrity number (RIN) > 4 and at least 0.1 µg of RNA were advanced to library preparation and sequencing. Libraries were prepared from RNA using the NEBNext Ultra II RNA Library Prep Kit for Illumina, which included poly-A enrichment using poly-T oligo-attached magnetic beads. mRNA was fragmented, and first-strand cDNA synthesis was performed using random hexamer primers, followed by second-strand cDNA synthesis. Sequencing was performed on the Illumina NovaSeq 6000 platform, generating 150 bp paired-end (PE150) reads for each sample. Extraction, library preparation, and sequencing was performed by Novogene Inc.

2.3 | Transcriptomic analysis

The quality of sequence files was assessed using the FastQC package[24] before and after trimming steps. Trimmomatic[25] (ILLUMINACLIP: TruSeq3-PE.fa:2:30:10:2:True, LEADING: 3, TRAILING: 3, SLIDINGWINDOW: 4:15, and MINLEN: 36) was used to remove adapter sequences and any sequences with low mean quality scores. Sequences were aligned to GRCh38 using STAR alignment[26] and count matrices were generated using featureCounts.[27] The count matrices were normalized using the counts per million (CPM) function in the edgeR package. Expression levels of positive control genes (*DBH*, *SLC6A2*, and *SLC6A3*) were checked to confirm accurate sampling. Cases with < 100 CPM of *DBH* or 10 CPM of *SLC6A2* in the LC, or < 100 CPM or *SLC6A3* in the SN were excluded from subsequent analyses.

Principal component analyses (PCA) were performed using the RunPCA command from the Seurat package in R with 20 principal components computed. Differential expression analyses were performed using the edgeR package.[28] Only genes with at least five counts present in at least 25% of samples were included in differential expression analyses. Multiple comparison correction was done using the Benhamini–Hochberg method[29] and the upper bound of the expected false discovery rate (FDR) is reported in analyses as the FDR. Differential expression analyses set cutoffs at 0.05 FDR and ± 0.5 log-fold change (logFC) to balance statistical significance with the need to detect changes limited to small cell populations in the bulk sample. The design matrix for differential expression analyses is formed from an additive model formula including the case. Differential expression analyses were done both with (corrected) and without (uncorrected) RIN as a covariate in the design formula.

Gene set enrichment analysis (GSEA) was done using the fgsea package[30] in R. The Hallmark gene set collection was downloaded from the GSEA Molecular Signatures Database.[31,32] The gene set files were filtered to contain only genes present in the differential expression table (5% FDR and ± 0.5 logFC) and then reformatted to the specifications required by the fgsea package. The differentially expressed genes (DEGs) were ranked based on the negative $\log_{10}(P \text{ value})$ such that the genes with the smallest *P* values were ranked at the very top of the ranking list. The fgsea function was run on the filtered gene set files with the ranked genes using a minimum gene set size of 10 and a maximum of 500.

2.4 | Immunohistochemistry

Formalin-fixed paraffin embedded tissue cut at 8 µm was cut from the pons at the level of the LC and the midbrain at the level of the SN for 13 *post mortem* cases (Table 2). Sections were deparaffinized and underwent antigen retrieval using the Discovery CC1 solution (950–500) for 40 minutes at 95°C. Sections were labeled with HMGCS1 (1:400, ab155787), ABCA1 (1:200, NB400-105), and LDLR (1:200, 10785-1-AP) developed with the Discovery Purple kit (760-229) and counterstained with hematoxylin, MYLIP (1:50, 15455-1-AP) developed with the Discovery Green HRP kit (760-721) and counterstained with hematoxylin, and SREBP2 (1:200, PA1338) developed with the Discovery Purple kit with no counterstaining. The OmniMap anti-Rabbit HRP (760-4311) was used for secondary detection of all primary antibodies. A set of serial LC slides run without primary antibody or counterstain were treated with the anti-Rabbit HRP secondary antibody and purple chromogen to verify SREBP2 labeling in the LC.

Immunostained sections were scanned using a Zeiss Axioscan slide scanner. Staining results were assessed semi-quantitatively by selecting 500 × 500 µm regions of interest and scoring all neurons within the frame on a scale from 0 to +++. A score of "+" was assigned to neurons exhibiting faint diffuse staining or, in the case of granular staining, a few speckles—differentiating them from neurons completely devoid of signal. A score of "++" indicated moderate-to-strong diffuse staining or speckled granular staining covering most, but not all, of the neuron. A score of "+++" was assigned to neurons displaying very strong diffuse staining or granular staining occupying the entire cell. These qualitative scores were converted into numerical values (0–3), the proportion of neurons at each score level was determined relative to the total neurons counted, and an average score was calculated for each nucleus in each case.

Scores were analyzed using a paired Wilcoxon test to compare average scores between nuclei for cases at Braak stage 0 to II and Braak stage VI.

3 | RESULTS

3.1 | Nucleus sampling

RNA sequencing data for paired LC and SN samples were available for 23 cases spanning Braak stages 0 through III (Table 1). To ensure accurate sampling, we analyzed CPM for *DBH*, *SLC6A2*, and *SLC6A3*. *DBH* encodes dopamine-β-hydroxylase, responsible for converting dopamine to noradrenaline, and *SLC6A2* encodes the norepinephrine transporter, both serving as LC markers. *SLC6A3*, encoding the dopamine transporter, was used as an SN marker. One case was excluded due to lower-than-expected CPM values for *DBH* and *SLC6A2*, indicative of incorrect LC sampling (Figure S2 in

TABLE 2 Demographics and case characteristics for the IHC study.

Case	Syndrome	Age	Sex	Thal phase	Braak stage	CERAD-NP score
11	Control	67	Female	0	0	None
12	Behavioral variant frontotemporal dementia	77	Female	4	0	Moderate
13	None	64	Female	2	I	Moderate
14	Amnestic mild cognitive impairment	81	Female	1	II	None
16	Control	84	Female	2	II	Mild
17	Control	64	Male	0	I	None
19	Dementia of AD	87	Male	3	II	Moderate
20	Dementia of AD	63	Male	5	VI	Severe
21	Dementia of AD	77	Male	5	VI	Severe
22	Dementia of AD	64	Male	5	VI	Severe
23	Dementia of AD	75	Female	5	VI	Severe
24	Dementia of AD	76	Female	5	VI	Severe
25	Dementia of AD	67	Female	5	VI	Severe

Abbreviations: AD, Alzheimer's disease; CERAD, Consortium to Establish a Registry for Alzheimer's Disease; IHC, immunohistochemistry; NP, neuropsychological battery.

supporting information). Transcript counts and the final cohort's CPM matrix are provided in Data S2 and S3, respectively, in supporting information.

3.2 | Demographics of cohort for transcriptomic analysis

Bulk mRNA sequencing was conducted for both LC and SN in the 22 cases meeting the criteria. Although an equal number of male and female cases were initially collected, RNA quality variations led to the exclusion of more female cases, resulting in a cohort with eight females (36%). Thus, while sex parity was intended, the final cohort over-represents males. Other demographic factors, including informant-reported race, are better balanced (Data S1). The average age of the cohort was 64 years (range 37–91). Six cases were Braak stage 0, four were Braak stage I, four were Braak stage II, and eight were Braak stage III (Table 2). Individual case details are found in Data S1.

3.3 | RNA and sequencing quality effects on computed gene expression

The median RIN score for the samples was 5.8, with a range of 4.1 to 7.3 (Data S1). To assess the impact of RNA quality on the results, we encoded the RIN scores onto a PCA applied to all sequenced samples (Figure S3 in supporting information). The RIN score, along with other inter-individual differences, appears to account for some of the variation observed along first principal component (PC-1). Notably, the top 10 genes loading on PC-1 are all mitochondrially encoded (Data S4 in supporting information), highlighting the influence of inter-individual variation in RNA quality on this principal component. Thus, RIN was included as a covariate in the design formula.

3.4 | Differential transcriptomic analysis between the LC and SN

We compared the transcriptomes of LC and SN samples to identify differences that may contribute to the selective vulnerability of the LC (Figure 1). In a PCA of all paired samples, LC and SN samples distinctly separated along the second principal component (PC-2). We then conducted differential expression analysis between the LC and SN on paired samples across Braak stages 0 to III, incorporating participant identifiers in the design formula to account for the matched sample design. Including RIN as a covariate, we identified 845 DEGs between the LC and SN in Braak stage 0 (Data S5 in supporting information), 1857 DEGs in Braak stage I (Data S6 in supporting information), 1981 DEGs in Braak stage II (Data S7 in supporting information), and 1036 DEGs in Braak stage III (Data S8; Figure S4 in supporting information). In contrast, without including RIN in the design formula, 3908 DEGs were identified in Braak stage 0 (Data S9 in supporting information), 3032 in Braak stage I (Data S10 in supporting information), 2164 in Braak stage II (Data S11 in supporting information), and 4984 in Braak stage III (Data S12 in supporting information; Figure S4). GSEA was performed on the RIN-corrected and uncorrected DEGs identified between the LC and SN for each Braak stage individually (Figure 2, Figures S5, S6 in supporting information). In Braak stage 0, the 845 RIN-corrected DEGs between the LC and SN showed significant enrichment in 16 of the 50 gene sets from the Hallmark pathways collection[32] (Figure 2A). In Braak stage III, the 1036 RIN-corrected DEGs showed significant enrichment in 12 of the 50 gene sets from the Hallmark pathways collection (Figure 2B). Upon examination on the

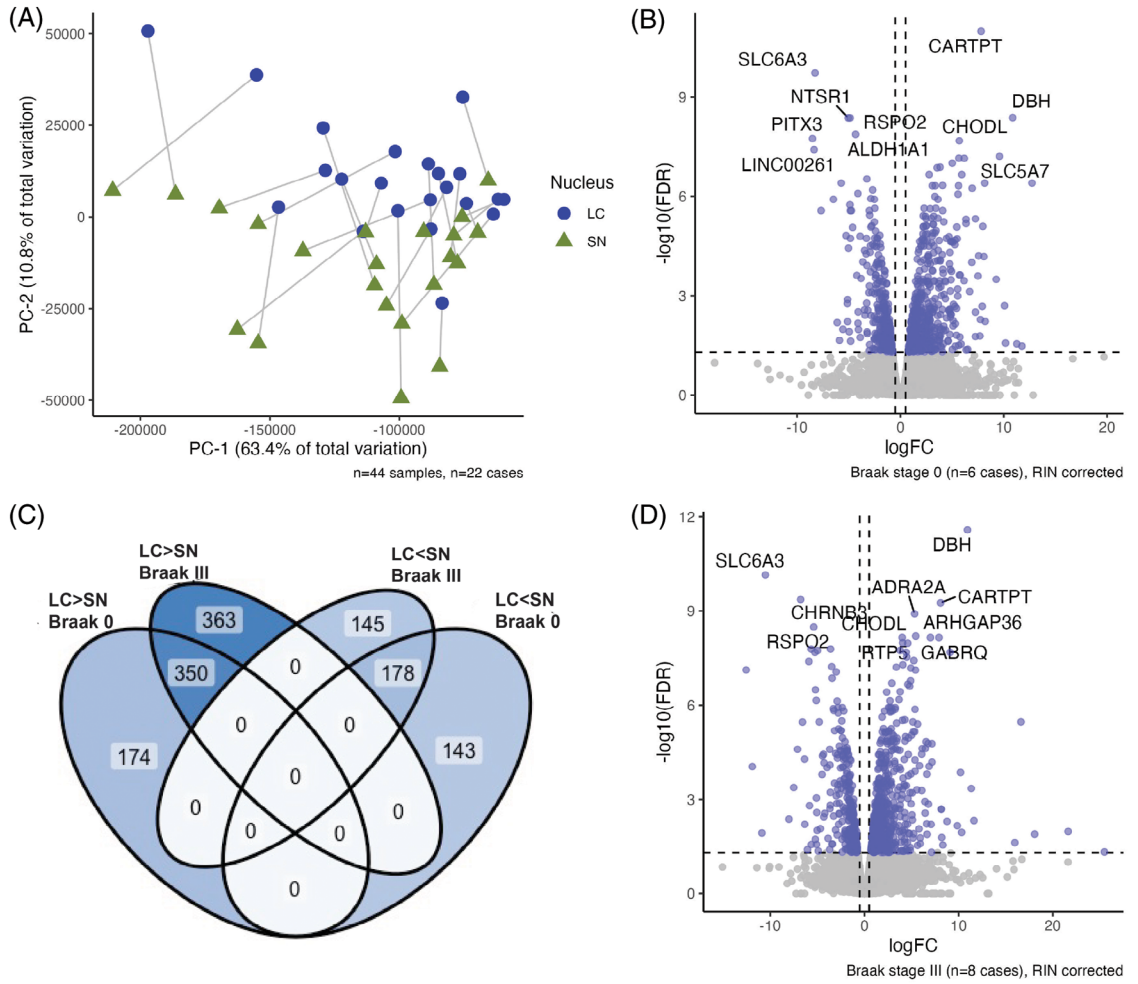

FIGURE 1 A, The matched LC and SN samples ($n = 22$) segregate along PC-2 in a PCA of gene expression for all matched samples. Connecting lines between points denote the case that both samples were collected from. B, There were 845 DEGs between the LC and SN in Braak stage 0 matched samples ($n = 6$, SN = baseline) in the RIN-corrected and 1036 DEGs in the Braak stage III matched samples ($n = 8$, SN = baseline) in the RIN-corrected model (D). C, Of the 524 genes more expressed in the LC than the SN in Braak 0, 350 remained more expressed in the LC in Braak III. Of the 321 genes more expressed in the SN than the LC in Braak 0, 178 remained more expressed in the SN than the LC in Braak III. DEG, differentially expressed gene; LC, locus coeruleus; logFC, log fold change; PC-2, principal component 2; PCA, principal component analysis; RIN, RNA integrity number; SN, substantia nigra

enriched gene sets maintained between Braak stage 0 and Braak stage III using the RIN-corrected DEGs, we focused subsequent analysis on the findings of apical junction enrichment, epithelial–mesenchymal transition enrichment, KRAS signaling, estrogen response, antioxidant pathways, and cholesterol homeostasis.

3.5 | Cholesterol regulation differs between the LC and SN at baseline

Because cholesterol homeostasis was a top hit in the GSEA, genes involved in cholesterol sensing and production were examined among Braak stage 0 cases. The selected genes included those coding proteins in the sterol regulatory element binding proteins (SREBP) and liver X receptor-retinoid X receptor (LXR/RXR) transcriptional axes, including the lanosterol and cholesterol producing pathways.[33–36] Of the 37 genes examined among Braak stage 0 cases, 6 had lower expression in the LC relative to the SN, 21 were more highly expressed in the LC than the SN, and 10 were not significantly differentially expressed (Figure 3). The 21 genes with significantly more expression in the LC than the SN were mostly involved in the SREBP-mediated processes of cholesterol production and influx. The six genes with lower expression in the LC than the SN were mostly involved in cholesterol transport and efflux (Figure 3), including apolipoprotein E (*APOE*). Two of the examined genes, *ABCA1* and *TM7SF2*, changed in expression levels in the LC between Braak stages 0 and III (Figure S7 in supporting information).

Based on the transcriptomic results suggesting enrichment for cholesterol homeostatic pathways, we performed immunohistochemistry (IHC) labeling of select markers to verify their differences at the protein level between LC and SN neurons. SREBP2 was selected for IHC evaluation given its role as a master regulator of sterol synthesis in the brain.[37] LDLR and ABCA1 have well-established roles

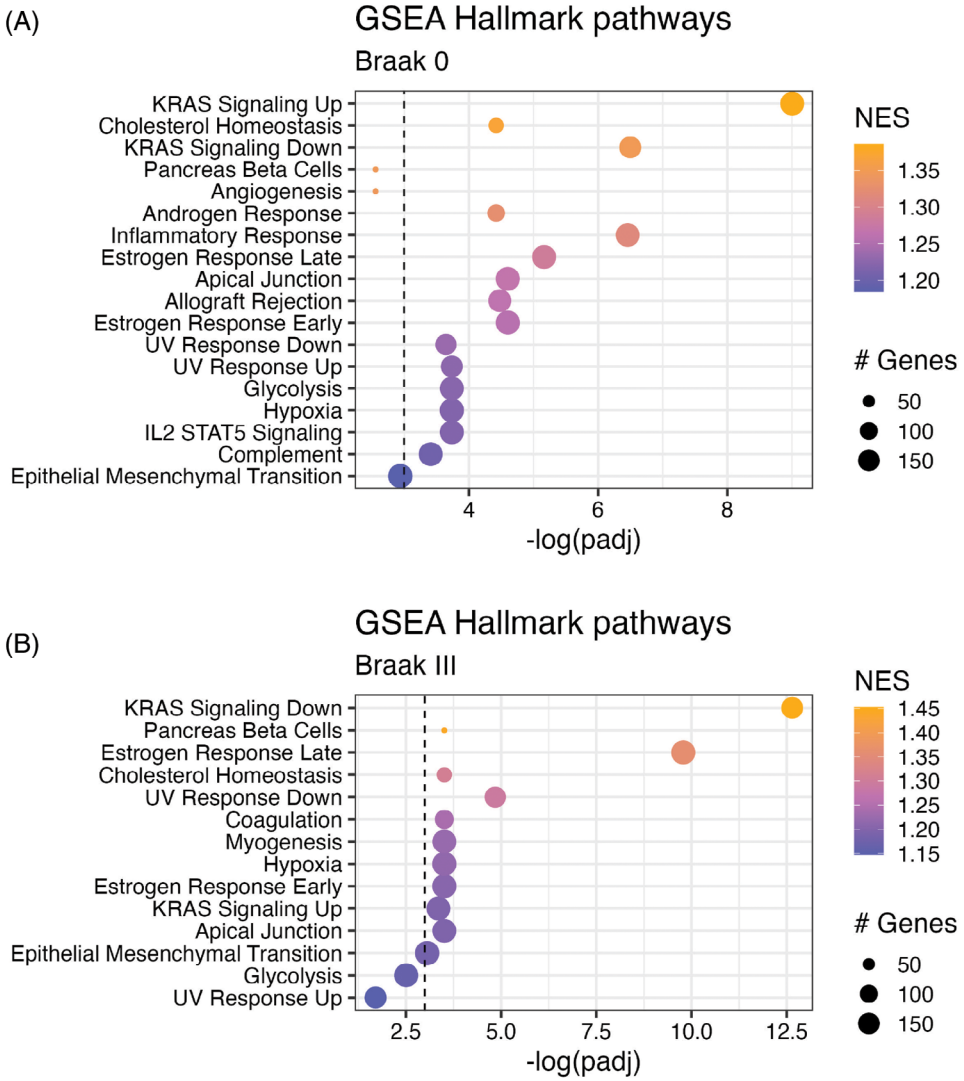

FIGURE 2 A, In Braak stage 0 cases, the RIN-corrected DEGs between the LC and SN showed statistically significant ($P_{adj} < 0.05$) enrichment for 16 Hallmark pathways. B, In Braak stage III cases, statistically significant enrichment was found for 12 Hallmark pathways. DEG, differentially expressed gene; GSEA, gene set enrichment analysis; LC, locus coeruleus; RIN, RNA integrity number; SN, substantia nigra

in Aβ metabolism and apoE lipidation,[38–40] and MYLIP is a selective E3 ubiquitin-protein ligase for LDLR,[41,42] making these three proteins priorities for IHC. Finally, we prioritized the lanosterol-producing pathway marker, HMGCS1, for IHC given that its dysregulation has been independently associated with AD pathogenesis by several groups.[34,43,44]

We identified significantly increased expression of LDLR in the LC relative to the SN at early (Braak stage 0–II) and late (Braak stage VI) AD neuropathologic stages (Figure 4). MYLIP was significantly more expressed in the SN than the LC in early (Braak stage 0–II) stage cases, but no statistically significant difference was observed in late-stage cases. The other proteins studied showed significant heterogeneity within the LC and SN and statistically significant differences were not detected. Of note, the quality of the inclusions for certain proteins, particularly ABCA1, was different between the LC and the SN. ABCA1 presented with a diffuse cytoplasmic staining in the LC, but as a more granular cytoplasmic staining in the SN (Figure 4C). The images analyzed for this study, as well as the counting regions of interest, are available on Dryad[45] and the counts are available in Data S13 in supporting information.

3.6 | Cell type composition differs between the LC and SN samples

Inflammatory pathways were among the top enriched pathways at both Braak stage 0 and Braak stage III differentiating the LC and SN. Given the nature of specimen collection, we considered the possibility that these differences might be partially due to variations in cell type composition. To explore this, we examined the differential expression of housekeeping genes for different nervous system cell types (Figure 5) and found evidence of differences in cell type composition

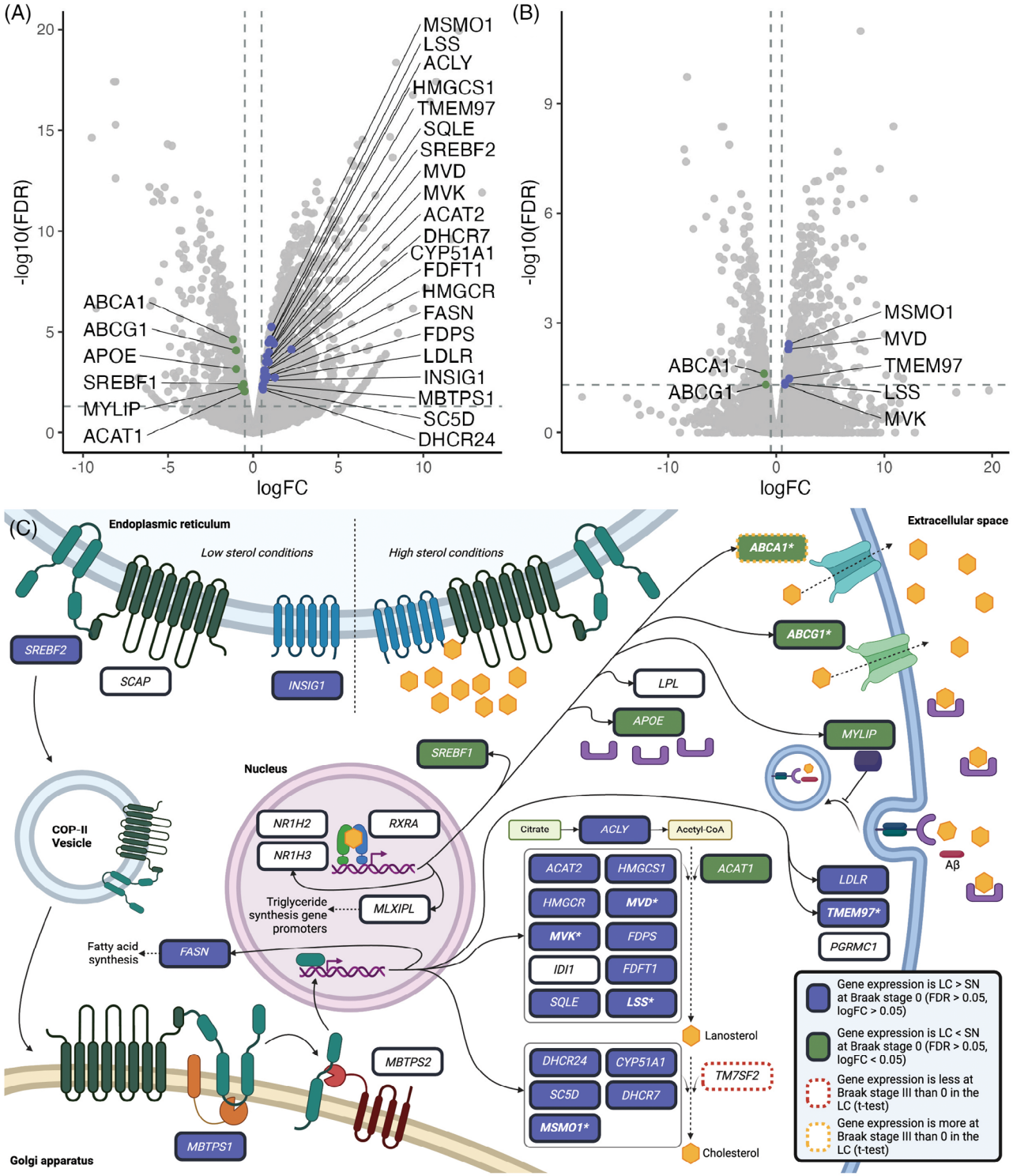

FIGURE 3 A list of 37 cholesterol-regulating or producing genes was examined among Braak stage 0 cases. A, In the uncorrected model of Braak stage 0 cases (SN = baseline), six genes (left-justified text, green dots) were less expressed in LC than in SN (logFC < −0.5; FDR < 0.05) and 21 genes (right-justified text, blue dots) were more expressed in LC than in SN (logFC > 0.5; FDR < 0.05). B, In the RIN-corrected model at Braak stage 0 (SN = baseline), two genes were less expressed in LC than in SN and five were more expressed in LC than in SN. C, The genes more expressed in LC at Braak stage 0 in the uncorrected model are mostly involved in SREBP-mediated production and influx of cholesterol. The genes less expressed in the LC at Braak stage 0 in the uncorrected model are mostly involved in LXR/RXR-mediated transport and efflux of cholesterol. FDR, false discovery rate; LC, locus coeruleus; logFC, log fold change; RIN, RNA integrity number; SN, substantia nigra

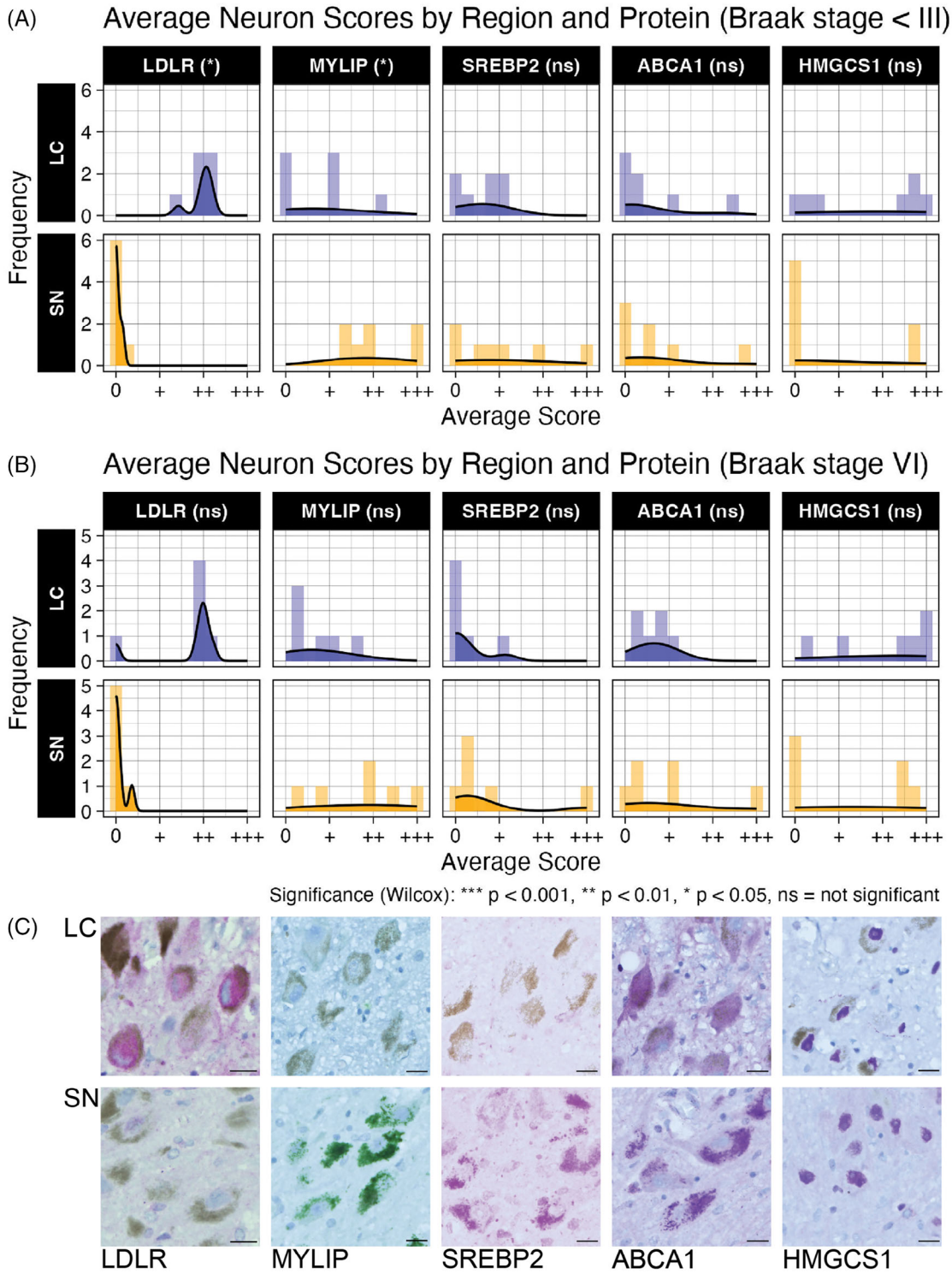

FIGURE 4 Five differentially expressed genes from cholesterol pathways were evaluated at the protein level using IHC and semi-quantitative assessment in Braak stage 0 to II (A) and Braak stage VI (B) cases. Neurons within a 500 × 500 μm region of interest were scored from 0 to +++. A numeric value was assigned to the scores (0 = 0, + to 1, ++ to 2, and +++ to 3) and each nucleus for each case received an average score. Paired Wilcoxon rank-sum tests without exact matching were used to test for statistically significant differences between the two nuclei. All markers evaluated had neuronal expression in at least one nucleus. Representative images (C) from a 67-year-old female at Braak stage 0 (Case #11, Table 2) are provided. Scale bars: 20 μm. IHC, Immunohistochemistry; LC, locus coeruleus; SN, substantia nigra

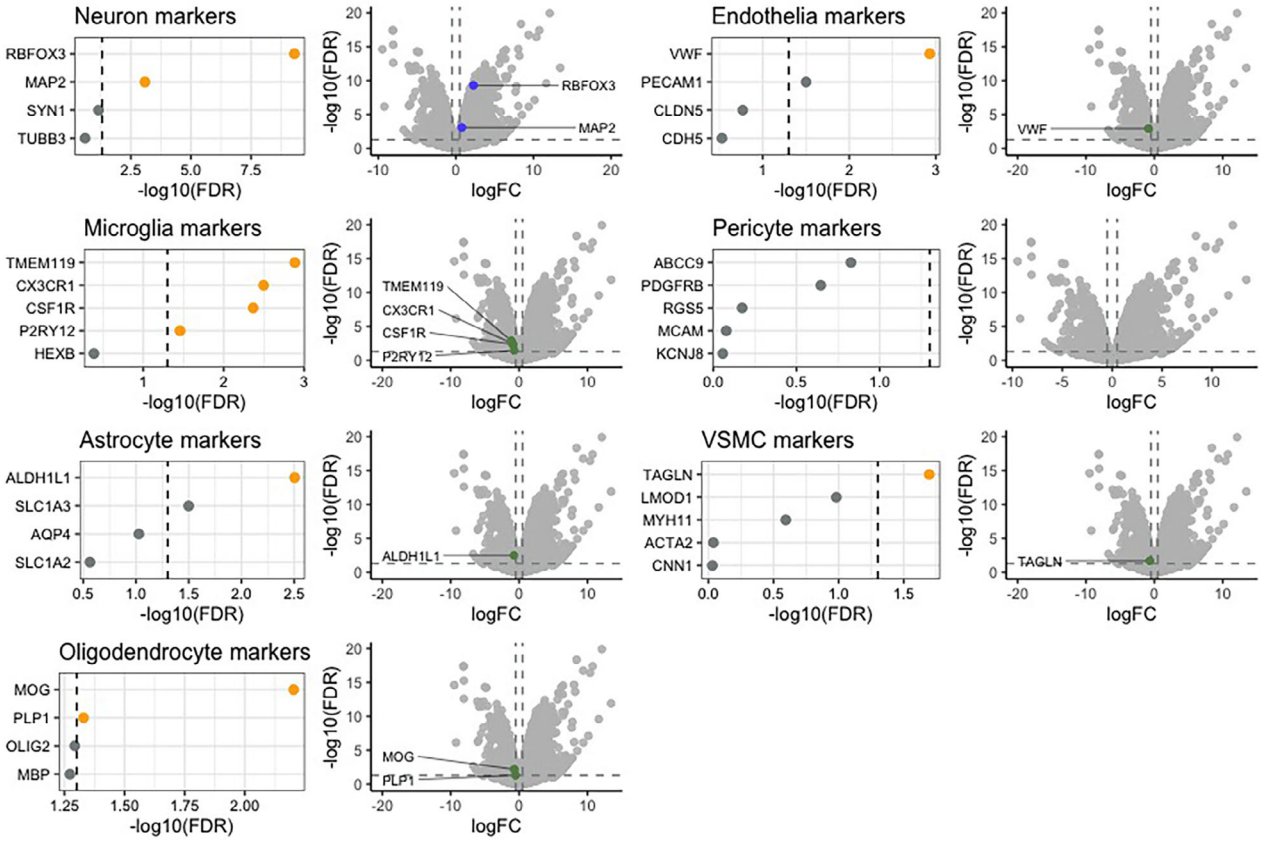

FIGURE 5 Genes encoding markers of microglia, astrocytes, oligodendrocytes, endothelial cells, pericytes, vascular smooth muscle cells, and neurons were examined in the uncorrected Braak stage 0 differential expression results in LC and SN (SN = baseline). Cutoffs for statistical significance include FDR of 0.05 and a logFC of 0.5. Genes passing these thresholds are denoted by yellow coloring in the dot plots and labeling in the volcano plots. FDR, false discovery rate; LC, locus coeruleus; logFC, log fold change; SN, substantia nigra; VSMC, vascular smooth muscle cells

between the LC and SN, particularly in microglia which had four of five markers more expressed in the SN.

Focusing on microglia differences (Figure S8 in supporting information), seven genes thought to be broad markers of the myeloid lineage are more expressed in the SN than the LC at Braak stage 0 in our uncorrected model. This further suggests that the SN samples may have included a higher proportion of microglia than the LC samples from the same cases. Three myeloid marker genes from Olah et al.[46]—*TENT5A*, *CD83*, and *TFRC*—were more highly expressed in the LC compared to the SN in both Braak stage 0 and III samples. These markers are linked to microglial clusters identified in prior single-cell mRNA sequencing studies.[46] Comparing Braak stage 0 and III LC samples, we observed increased average transcript levels of *FCN1* and *VCAN* (monocyte markers) as well as *CD3E* (a T-cell marker) in the higher Braak stage.

Given the likely cell composition differences between our samples, we refrained from in-depth examination of enriched pathways that would be strongly influenced by cell composition of the bulk samples. Apical junction genes (Figure S9 in supporting information) are associated with cell–cell adhesion and polarity, characteristic of ependymal cells and blood–brain barrier cells. Because the LC and SN are highly vascularized nuclei,[47,48] sampling variations may significantly contribute to this enrichment. The leading-edge genes contributing to apical junction enrichment at Braak stage 0 (Figure S9) suggest that non-vascular factors may be contributing to its enrichment though. Several of the leading-edge genes, including *CALB2*, *SLC30A3*, *NEGR1*, and *CDH8* are mainly expressed by neurons[49] and hint at factors underlying neuronal specialization between the LC and SN.

Epithelial–mesenchymal transition enrichment in the brain is typically associated with morphogenic signaling in gliomas.[50] The leading-edge genes underlying this gene set (Figure S10 in supporting information) can be explained by other factors more germane to neurodegenerative diseases, too. For example, *SPOCK1*, *COL7A1*, and *VCAN* are also involved in extracellular matrix organization and cell–matrix interactions and have been implicated in AD.[51,52]

While we are refraining from analyzing pathways likely to be enriched due to cell composition differences, these preliminary results merit re-examination—particularly as additional single-cell resolution datasets for the LC and SN become available.

3.7 | KRAS signaling in the LC and SN

Our analysis revealed an enrichment of genes both upregulated and downregulated by KRAS signaling. To investigate potential differential regulation of KRAS between LC and SN, we examined various

KRAS regulators and effectors (Figure S11 in supporting information). We failed to detect systematic differences in the expression of KRAS activators, such as receptor tyrosine kinases and guanine nucleotide exchange factors, between nuclei. However, three genes encoding GTPase-activating proteins (GAPs)—*RASA1*, *RASA2*, and *NF1*—which facilitate the inactivation of KRAS by accelerating the hydrolysis of GTP to GDP,[53] exhibited higher expression levels in the LC at Braak stage 0. This might suggest a potential mechanism for reduced KRAS activity in the LC compared to the SN. Notably, we did not find significantly increased expression of KRAS inhibitors in the SN relative to the LC at Braak stage 0.

3.8 | Estrogen receptor signaling in the LC

Due to the enrichment of genes associated with estrogen signaling in our DEGs, we examined the expression levels of genes encoding estrogen receptors, coactivators, corepressors, and enhancers (Figure S12A, SB in supporting information). The uncorrected DEGs at Braak stage 0 feature increased expression of *ESR2* in the LC and increased expression of *PGR* and *SHGB* in the SN. This suggests that the SN is more specialized for response to progesterone signaling and that the LC is more specialized for response to estrogen signaling via estrogen receptor β. The LC also showed increased *ESR1* expression in Braak stage III relative to Braak stage 0 (Figure S12C). The RIN-corrected DEGs at Braak stage 0 only feature increased expression of *FOXA1* in the SN, a gene encoding a pioneer factor facilitating estrogen receptor binding to chromatin.

3.9 | Antioxidant pathway differences differ between the LC and SN

Because there was enrichment for redox-related pathways in the GSEA (e.g., hypoxia, ultraviolet response), the DEGs between the LC and SN at Braak stage 0 and III (Figure 6) were examined to identify those appearing on a list of 63 antioxidant genes compiled by Gelain et al.[54] At Braak stage 0, 7 of the 63 antioxidant genes were more expressed in the SN than the LC. Of these seven genes, five were genes encoding metallothionein proteins. The remaining two included a peroxidase-encoding gene, *LPO*, and a superoxidase dismutase, *SOD3*. In contrast, there were only three of the antioxidant genes more expressed in the LC than the SN at Braak stage 0—two thioredoxin domain proteins and a peroxidase, *MPO*.

Of note, there were no genes encoding the metallothionein proteins examined here identified as DEGs more expressed in the LC than the SN. Similarly, there were no genes encoding the thioredoxin domain proteins examined here identified as more expressed DEGs in the SN than the LC. While the DEGs are functionally segregated in this regard, there is some degree of expression of both metallothionein genes (Figure 6) and thioredoxin domain genes in both nuclei (Figure S13 in supporting information).

4 | DISCUSSION

In this study, we sought to investigate pathways contributing to the augmented vulnerability of the LC to AD-related degeneration at early stages. We analyzed paired *post mortem* samples from the LC and SN in individuals with early AD, specifically Braak stages 0 to III. Despite their similar structures and shared susceptibility to synucleinopathies and accumulation of AD tau from Braak 0, we found significant differences in gene expression between the LC and SN even at Braak stage 0. Notably, differences in cholesterol homeostasis and antioxidant-related genes may contribute to LC's greater vulnerability to degeneration in AD compared to the SN.

Gene expression comparisons between the LC and SN revealed substantial differences both at baseline (Braak stage 0) and during intermediate stages of AD progression (Braak stage III). Given the extensive number of DEGs identified at these stages, GSEA was used to pinpoint pathways that distinguish the two nuclei.

Cholesterol synthesis and maintenance consistently emerged as key factors differentiating the LC and SN across the examined Braak stages. The LC showed a baseline (i.e., Braak stage 0) gene expression pattern suggestive of a higher demand for cholesterol compared to the SN. This may be met by upregulating the SREBP transcriptional axis, which enhances cholesterol production and influx, while downregulating the LXR/RXR transcriptional axis, which reduces cholesterol efflux. This pattern was corroborated by IHC labeling in LC and SN neurons, particularly of SREBP axis proteins such as LDLR. While disruptions in cholesterol synthesis and maintenance are well-established contributors to AD,[56–58] our findings were unexpected because the LC and SN share similar characteristics, such as large neuronal sizes and extensive projections throughout the brain.

There are several ways that differential expression of cholesterol homeostatic pathways might cause differential vulnerability to AD. Approximately one fifth of the body's cholesterol is in the brain, primarily within myelin sheaths.[33,59] The remaining brain cholesterol is largely found in astrocytic and neuronal plasma membranes, where it plays a crucial role in maintaining cell structure and synaptic transmission. Unlike the days-long half-life of circulating cholesterol in the body, cholesterol in the adult brain has a half-life ranging from months to years.[60] Because the brain is largely isolated from the peripheral cholesterol supply, it relies on its own synthesis to meet its needs. Dysregulation or deterioration of the LC's capacity to produce and maintain sufficient cholesterol levels could lead to neuronal loss in AD. This hypothesis is supported by findings from Varma et al. who reported reduced cholesterol production in AD.[34] Remarkably, Varma et al. did not observe these differences in LBD cases, in which the LC and SN are similarly vulnerable. We found decreased expression of *APOE* and *ABCA1* mRNA in the LC relative to the SN. The *APOE* gene, with its minor allele, *APOE* ε4, is a major genetic risk factor for sporadic AD.[61,62] *APOE* was among the DEGs between the LC and SN at baseline (Braak stage 0) with lower *APOE* mRNA levels detected in the LC. ABCA1 has protective effects in AD, likely through its role in reducing apoE lipidation and subsequent Aβ deposition.[40,63]

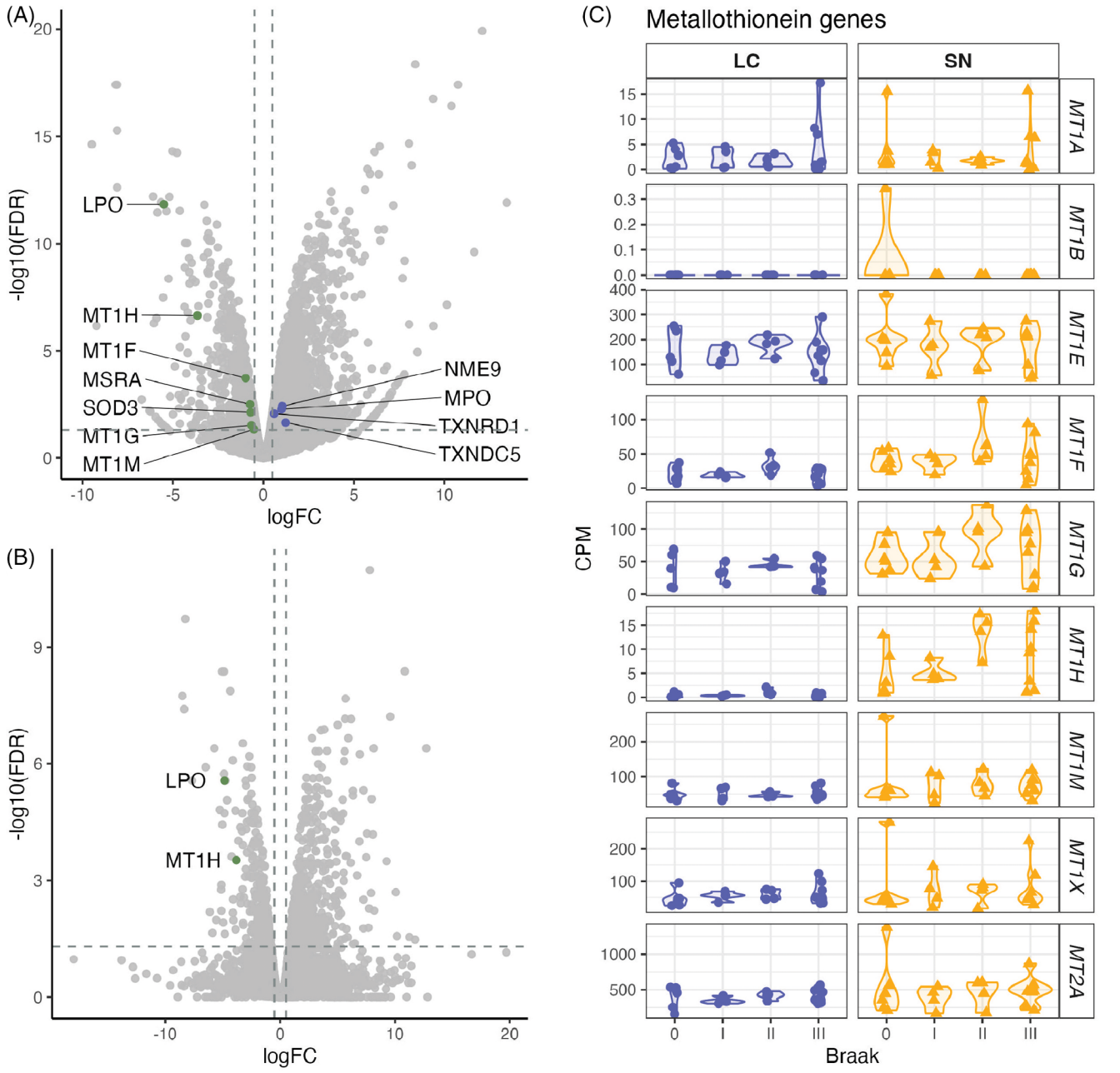

FIGURE 6 Differential expression of genes in LC and SN (logFC > 0 indicates greater expression of a gene in the LC). Cutoffs for significance are FDR < 0.05 and logFC > 0.5 or < −0.5. A–B, Significantly differentially expressed genes representing antioxidant enzymes or antioxidant activity selected from Gelain et al.[54] are labeled for analyses of cases at Braak stage 0 in uncorrected (A) and RIN-corrected (B) models. C, Metallothionein genes listed in Gelain et al. are expressed in both the LC and SN, with some more expressed in the SN relative to the LC. SN = baseline. FDR, false discovery rate; LC, locus coeruleus; logFC, log fold change; RIN, RNA integrity number; SN, substantia nigra

Additionally, in our RIN-uncorrected model, we observed significantly lower expression of *MYLIP* in the LC compared to the SN, alongside higher expression of *LDLR* and *TMEM97*. Together with PGRMC1, LDLR and TMEM97 form the Sigma-2 receptor trimeric complex at the cell membrane. Sigma-2 receptors internalize extracellular lipoproteins such as low-density lipoprotein and apoE, but can also internalize toxic Aβ oligomers.[38,39] IDOL, encoded by *MYLIP*, is an E3-ubiquitin ligase that degrades LDLR, thereby negatively regulating sigma-2 receptor expression.[41] The gene expression pattern observed here together with previous work[38,39,64] suggests that even at Braak stage 0, the LC may have a greater capacity to internalize toxic Aβ oligomers than the SN. Collectively, dysfunction in cholesterol homeostasis and the potential Aβ-related negative effects of cholesterol internalization machinery may represent an AD-specific mechanism underlying the selective vulnerability of the LC.

We specifically examined antioxidant-related genes to explore how differences in metabolism might contribute to the differential vulnerability of the LC versus SN. Using a set of genes identified by

Gelain et al.,[54] we found that, at baseline, the SN is enriched for genes encoding metallothionein proteins. Metallothionein genes, known for their high cysteine content,[65] play roles beyond antioxidant activity, including the regulation of essential metals and protection against metal toxicity. Heavy metal accumulation is believed to contribute to neurodegeneration in both AD and other neurodegenerative diseases, such as LBD.[66,67] Both the LC and SN contain neuromelanin, making them particularly susceptible to heavy metal accumulation;[66] however, some evidence suggests that the LC may be more vulnerable to heavy metal accumulation than the SN.[68,69] This difference could be explained by the differential expression of metallothionein genes. Higher expression of metallothionein genes in the cortex has been highlighted as a resilience factor between individuals, which is reflected by the inter-regional pattern of vulnerability and resilience to AD in the SN and LC.[70]

Of note, we also found enrichment in genes downstream of KRAS activation and estrogen response. Examination of genes encoding regulators and components of KRAS did not reveal systematic differences between the LC and SN with obvious connections to selective vulnerability between the two. We detected differences between the LC and SN in estrogen and progesterone receptors, suggesting that the two regions may have different strategies for neuronal survival. Previous work has shown that the highest concentration of estrogen receptors in the brainstem is in the LC with specific implications for estrogen receptor-β LC expression and neuropsychiatric symptoms.[71]

Apical junction and epithelial–mesenchymal transition genes were also among the top enriched pathways differentiating DEGs between the LC and SN. Many genes associated with the apical junction and epithelial-mesenchymal transition are pleiotropic. For example, *CALB2* is a marker of inhibitory neurons and has been identified in neuron populations immediately proximal to the LC in previous work.[72] Immune system and inflammatory-associated pathways were enriched in our DEGs. While there may be differences in the baseline activation of neuroinflammatory pathways between these regions, it is challenging to determine whether these differences reflect true variations in inflammatory activity or simply differences in cell composition. Consistent with this possibility, we found evidence of increased relative composition of glia in the SN and increased relative composition of neurons in the LC (Figure 5). There were, however, three microglial clusters identified in previous single-cell transcriptomic studies that showed stronger signals in the LC.[46] Additionally, there seems to be an increase in microglial markers in the LC from Braak stage 0 to III, suggesting a potential upregulation of inflammatory activity as AD progresses. These early neuroinflammatory patterns are consistent with evidence of neuropathologic tau lesions within the LC at these stages.[5,6] Further studies should examine the relationship between pathological hallmarks of AD and the neuroinflammatory markers identified here in the LC.

Our study leverages the strengths of human *post mortem* tissue analysis while addressing the inherent limitations of its cross-sectional nature. By analyzing matched samples from contrasting brain regions within the same individuals, we minimized the effects of unavoidable biological (e.g., age, sex) and technical (e.g., periagonal events, *post mortem* interval) inter-individual variability that can significantly influence results. This approach enhances our ability to detect region-specific differences and provides more robust insights into disease progression, despite the imprecision of using Braak staging to model disease processes. Additionally, we mitigated potential confounding factors by excluding cases with co-pathologies and using well-characterized tissue from individuals at early disease stages. Although our data are interpreted at the bulk transcriptional level—an approach chosen to include more participants due to the technical and financial constraints of single-cell "omics"—we refrained from making inferences potentially affected by cell composition, which ideally would be examined through single-cell platforms, as demonstrated by Weber et al. for the LC.[72] We strengthen the validity of portions of our transcriptomic results by investigating findings using IHC, allowing us to resolve findings at the cell-type level. These strategies collectively maximize the robustness and specificity of our findings. Nevertheless, caution should be taken in the interpretation of bulk transcriptomic data alone.

We have identified key differences in cholesterol homeostasis, heavy metal processing, and other gene sets that may contribute to the baseline vulnerability of the LC and SN in AD. These findings highlight potential therapeutic targets, pending further mechanistic verification. In particular, the potential that enrichment for cholesterol transport machinery in the LC might increase its susceptibility to toxic Aβ oligomers warrants further study. The ability to model processes in the LC and SN has advanced significantly in recent years, with transgenic mouse models allowing inducible control of gene expression in dopaminergic and noradrenergic neurons.[73,74] In vitro modeling of LC and SN neurons is even now feasible using human pluripotent stem cells.[75] These platforms provide valuable tools for rigorously testing hypotheses generated from datasets like ours. A deeper understanding of the causal factors driving LC degeneration and strategies to modify its vulnerability could have a profound impact on the treatment of AD and other neurodegenerative and stress-related disorders.

ACKNOWLEDGMENTS

The authors thank the research participants and families at the Biobank for Aging Studies at the University of São Paulo and the University of California, San Francisco Memory and Aging Center for their contributions to this work. We also thank the staff of the São Paulo Autopsy Service and UCSF Neurodegenerative Disease Brain Bank, particularly Tâmara Galvez, Levi Dias, Wing Hung Lee, Tia LaMore, and Sula Perloff, without whom this work would not be possible. Additionally, we thank the staff of the UCSF high-performance compute cluster (Wynton) and the Grinberg lab for their technical and administrative assistance with this work. The authors also thank Dr. Peter Sudmant and Dr. José Pablo Vázquez-Medina for their guidance on technical and intellectual aspects of this project. Some figures here were created with BioRender.com. This study was supported by the Rainwater Charitable Foundation, NIH P30 AG062422, NIH T32 GM139780, NIA K24 AG053435, NIA R01 AG064314, NIA R01 AG060477, NIA R01 AG075802, UC Berkeley Greater Good Science Center, Fundacao de Apoio a Pesquisa do Estado de São Paulo

(06/55318, 2009/09134-4, and 2012/07526-5), and the Alzheimer's Association (AARG-20-678884).

CONFLICT OF INTEREST STATEMENT

A.J.E. has no relevant competing financial interests with this manuscript. A.J.E. serves as an unpaid steering committee member for the Genomic Answers for Children's Health Alliance at Leavitt Partners and as an unpaid executive committee member for the Neuromodulatory Subcortical System's Professional Interests Area of the International Society to Advance Alzheimer's Research and Treatment. S.T. has no relevant competing interests with this manuscript, but is co-founder of Luxa Biotech developing an RPE therapy for AMD and has patents related to RPE cell therapy: Retinal pigment epithelial stem cells, Patent number: 8481313; Methods of treating a retinal disease by Retinal pigment epithelial stem cells, Patent number: 10034916; S.T. has advised BlueRock Therapeutics, Vita Therapeutics, and SANA Biotechnology. All other authors have no declared conflicts of interest to declare. Author disclosures are available in the Supporting Information.

DATA AVAILABILITY STATEMENT

The transcriptomic data discussed in this publication have been deposited in NCBI's Gene Expression Omnibus[55] and are accessible through GEO Series accession number GSE273787. Processed transcriptomic data, metadata, photomicrographs, and Supplementary Data are available on Dryad.[45]

CONSENT STATEMENT

Informed consent was collected from the participant's next of kin or a durable power of attorney, consistent with the site-specific approved protocol at the University of São Paulo or University of California, San Francisco.

ORCID

Alexander J. Ehrenberg https://orcid.org/0000-0003-4334-9424
Lea T. Grinberg https://orcid.org/0000-0002-6809-0618

REFERENCES

1. Rub U, Stratmann K, Heinsen H, et al. The brainstem tau cytoskeletal pathology of Alzheimer's disease: a brief historical overview and description of its anatomical distribution pattern, evolutional features, pathogenetic and clinical relevance. *Curr Alzheimer Res*. 2016;13(10):1178-1197. doi:10.2174/1567205013666160606100509
2. Stratmann K, Heinsen H, Korf HW, et al. Precortical phase of Alzheimer's disease (AD)-Related tau cytoskeletal pathology. *Brain Pathol*. 2016;26(3):371-386. doi:10.1111/bpa.12289
3. Attems J, Thomas A, Jellinger K. Correlations between cortical and subcortical tau pathology. *Neuropath Appl Neuro*. 2012;38(6):582-590. doi:10.1111/j.1365-2990.2011.01244.x
4. Ehrenberg AJ, Kelberman MA, Liu KY, et al. Priorities for research on neuromodulatory subcortical systems in Alzheimer's disease: position paper from the NSS PIA of ISTAART. *Alzheimers Dement*. 2023;19(5):2182-2196. doi:10.1002/alz.12937
5. Ehrenberg AJ, Nguy AK, Theofilas P, et al. Quantifying the accretion of hyperphosphorylated tau in the locus coeruleus and dorsal raphe nucleus: the pathological building blocks of early Alzheimer's disease. *Neuropathol Appl Neurobiol*. 2017;43(5):393-408. doi:10.1111/nan.12387
6. Andres-Benito P, Fernandez-Duenas V, Carmona M, et al. Locus coeruleus at asymptomatic early and middle Braak stages of neurofibrillary tangle pathology. *Neuropathol Appl Neurobiol*. 2017;43(5):373-392. doi:10.1111/nan.12386
7. Braak H, Thal DR, Ghebremedhin E, Del Tredici K. Stages of the pathologic process in Alzheimer disease: age categories from 1 to 100 years. *J Neuropathol Exp Neurol*. 2011;70(11):960-969. doi:10.1097/NEN.0b013e318232a379
8. Jacobs HIL, Becker JA, Kwong K, et al. In vivo and neuropathology data support locus coeruleus integrity as indicator of Alzheimer's disease pathology and cognitive decline. *Sci Transl Med*. 2021;13(612):eabj2511. doi:10.1126/scitranslmed.abj2511
9. Theofilas P, Ehrenberg AJ, Dunlop S, et al. Locus coeruleus volume and cell population changes during Alzheimer's disease progression: a stereological study in human postmortem brains with potential implication for early-stage biomarker discovery. *Alzheimers Dement*. 2017;13(3):236-246. doi:10.1016/j.jalz.2016.06.2362
10. Jacobs HIL, Riphagen JM, Ramakers I, Verhey FRJ. Alzheimer's disease pathology: pathways between central norepinephrine activity, memory, and neuropsychiatric symptoms. *Mol Psychiatry*. 2021;26:897-906. doi:10.1038/s41380-019-0437-x
11. Ehrenberg AJ, Suemoto CK, Franca Resende EP, et al. Neuropathologic correlates of psychiatric symptoms in Alzheimer's disease. *J Alzheimers Dis*. 2018;66(1):115-126. doi:10.3233/JAD-180688
12. Oh J, Eser RA, Ehrenberg AJ, et al. Profound degeneration of wake-promoting neurons in Alzheimer's disease. *Alzheimers Dement*. 2019;15(10):1253-1263. doi:10.1016/j.jalz.2019.06.3916
13. Betts MJ, Kirilina E, Otaduy MCG, et al. Locus coeruleus imaging as a biomarker for noradrenergic dysfunction in neurodegenerative diseases. *Brain*. 2019;142(9):2558-2571. doi:10.1093/brain/awz193
14. Bueicheku E, Diez I, Kim CM, et al. Spatiotemporal patterns of locus coeruleus integrity predict cortical tau and cognition. *Nat Aging*. 2024;4(5):625-637. doi:10.1038/s43587-024-00626-y
15. Ramon-Moliner E, Nauta WJ. The isodendritic core of the brain stem. *J Comp Neurol*. 1966;126(3):311-335. doi:10.1002/cne.901260301
16. Grofova I, Deniau JM, Kitai ST. Morphology of the substantia nigra pars reticulata projection neurons intracellularly labeled with HRP. *J Comp Neurol*. 1982;208(4):352-368. doi:10.1002/cne.902080406
17. Parvizi J, Van Hoesen GW, Damasio A. The selective vulnerability of brainstem nuclei to Alzheimer's disease. *Ann Neurol*. 2001;49(1):53-66. doi:10.1002/1531-8249(200101)49:1⟨53::aid-ana30⟩3.0.co;2-q
18. Suemoto CK, Ferretti-Rebustini RE, Rodriguez RD, et al. Neuropathological diagnoses and clinical correlates in older adults in Brazil: a cross-sectional study. *PLoS Med*. 2017;14(3):e1002267. doi:10.1371/journal.pmed.1002267
19. Spina S, La Joie R, Petersen C, et al. Comorbid neuropathological diagnoses in early versus late-onset Alzheimer's disease. *Brain*. 2021;144(7):2186-2198. doi:10.1093/brain/awab099
20. Montine TJ, Phelps CH, Beach TG, et al. National Institute on Aging-Alzheimer's Association guidelines for the neuropathologic assessment of Alzheimer's disease: a practical approach. *Acta Neuropathol*. 2012;123(1):1-11. doi:10.1007/s00401-011-0910-3
21. Mackenzie IR, Neumann M, Baborie A, et al. A harmonized classification system for FTLD-TDP pathology. *Acta Neuropathol*. 2011;122(1):111-113. doi:10.1007/s00401-011-0845-8
22. McKeith IG, Dickson DW, Lowe J, et al. Diagnosis and management of dementia with Lewy bodies: third report of the DLB Consortium. *Neurology*. 2005;65(12):1863-1872. doi:10.1212/01.wnl.0000187889.17253.b1
23. McKee AC, Cairns NJ, Dickson DW, et al. The first NINDS/NIBIB consensus meeting to define neuropathological criteria for the diagnosis of chronic traumatic encephalopathy. *Acta Neuropathol*. 2016;131(1):75-86. doi:10.1007/s00401-015-1515-z

24. Babhraham Bioinformatics. *FastQC: A Quality Control Tool for High Throughput Sequence Data*. Babhraham Bioinformatics; 2010. http://www.bioinformatics.babraham.ac.uk/projects/fastqc/
25. Bolger AM, Lohse M, Usadel B. Trimmomatic: a flexible trimmer for Illumina sequence data. *Bioinformatics*. 2014;30(15):2114-2120. doi:10.1093/bioinformatics/btu170
26. Dobin A, Davis CA, Schlesinger F, et al. STAR: ultrafast universal RNA-seq aligner. *Bioinformatics*. 2013;29(1):15-21. doi:10.1093/bioinformatics/bts635
27. Liao Y, Smyth GK, Shi W. featureCounts: an efficient general purpose program for assigning sequence reads to genomic features. *Bioinformatics*. 2014;30(7):923-930. doi:10.1093/bioinformatics/btt656
28. Robinson MD, McCarthy DJ, Smyth GK. edgeR: a Bioconductor package for differential expression analysis of digital gene expression data. *Bioinformatics*. 2010;26(1):139-140. doi:10.1093/bioinformatics/btp616
29. Benjamini Y, Hochberg Y. Controlling the false discovery rate: a practical and powerful approach to multiple testing. *J R Stat*. 1995;57(1):289-300.
30. Korotkevich G, Sukhov V, Sergushichev A. Fast gene set enrichment analysis. *bioRxiv*. 2019:060012. doi:10.1101/060012
31. Subramanian A, Tamayo P, Mootha VK, et al. Gene set enrichment analysis: a knowledge-based approach for interpreting genome-wide expression profiles. *Proc Natl Acad Sci U S A*. 2005;102(43):15545-15550. doi:10.1073/pnas.0506580102
32. Liberzon A, Birger C, Thorvaldsdottir H, Ghandi M, Mesirov JP, Tamayo P. The Molecular Signatures Database (MSigDB) hallmark gene set collection. *Cell Syst*. 2015;1(6):417-425. doi:10.1016/j.cels.2015.12.004
33. Dietschy JM, Turley SD. Thematic review series: brain lipids. Cholesterol metabolism in the central nervous system during early development and in the mature animal. *J Lipid Res*. 2004;45(8):1375-1397. doi:10.1194/jlr.R400004-JLR200
34. Varma VR, Busra Luleci H, Oommen AM, et al. Abnormal brain cholesterol homeostasis in Alzheimer's disease-a targeted metabolomic and transcriptomic study. *NPJ Aging Mech Dis*. 2021;7(1):11. doi:10.1038/s41514-021-00064-9
35. Rawson RB. The SREBP pathway–insights from Insigs and insects. *Nat Rev Mol Cell Biol*. 2003;4(8):631-640. doi:10.1038/nrm1174
36. Lee SH, Lee JH, Im SS. The cellular function of SCAP in metabolic signaling. *Exp Mol Med*. 2020;52(5):724-729. doi:10.1038/s12276-020-0430-0
37. Madison BB. Srebp2: a master regulator of sterol and fatty acid synthesis. *J Lipid Res*. 2016;57(3):333-335. doi:10.1194/jlr.C066712
38. Riad A, Lengyel-Zhand Z, Zeng C, et al. The sigma-2 receptor/TMEM97, PGRMC1, and LDL receptor complex are responsible for the cellular uptake of abeta42 and its protein aggregates. *Mol Neurobiol*. 2020;57(9):3803-3813. doi:10.1007/s12035-020-01988-1
39. Colom-Cadena M, Toombs J, Simzer E, et al. Transmembrane protein 97 is a potential synaptic amyloid beta receptor in human Alzheimer's disease. *Acta Neuropathol*. 2024;147(1):32. doi:10.1007/s00401-023-02679-6
40. Wahrle SE, Jiang H, Parsadanian M, et al. Overexpression of ABCA1 reduces amyloid deposition in the PDAPP mouse model of Alzheimer disease. *J Clin Invest*. 2008;118(2):671-682. doi:10.1172/JCI33622
41. Zelcer N, Hong C, Boyadjian R, Tontonoz P. LXR regulates cholesterol uptake through idol-dependent ubiquitination of the LDL receptor. *Science*. 2009;325(5936):100-104. doi:10.1126/science.1168974
42. Zhang CP, Tian Y, Zhang M, Tuo QH, Chen JX, Liao DF. IDOL, inducible degrader of low-density lipoprotein receptor, serves as a potential therapeutic target for dyslipidemia. *Med Hypotheses*. 2016;86:138-142. doi:10.1016/j.mehy.2015.11.010
43. Li Y, Bai H, Huang H, Zhu M, Zhang D, Huang X. Forward genetic screening of a novel gene hmgs-1 involved in Alzheimer disease pathogenesis in a transgenic caenorhabditis elegans model. *Biochem Biophys Res Commun*. 2020. doi:10.1016/j.bbrc.2020.02.076
44. Glasauer SMK, Goderie SK, Rauch JN, et al. Human tau mutations in cerebral organoids induce a progressive dyshomeostasis of cholesterol. *Stem Cell Reports*. 2022;17(9):2127-2140. doi:10.1016/j.stemcr.2022.07.011
45. Ehrenberg A, Sant C, Pereira F, et al. Pathways underlying selective neuronal vulnerability in Alzheimer's disease: contrasting the vulnerable locus coeruleus to the resilient substantia nigra [Dataset]. 2025; doi:10.5061/dryad.sbcc2frgp
46. Olah M, Menon V, Habib N, et al. Single cell RNA sequencing of human microglia uncovers a subset associated with Alzheimer's disease. *Nat Commun*. 2020;11(1):6129. doi:10.1038/s41467-020-19737-2
47. Finley KH. Angio-architecture of the substantia nigra and its pathogenic significance. *Arch Neurol Psychiatry*. 1936;36(1):118-127. doi:10.1001/archneurpsyc.1936.02260070126010
48. Finley KH, Cobb S. The capillary bed of the locus coeruleus. *J Comp Neurol*. 1940;73(1):49-58. doi:10.1002/cne.900730105
49. Zhang Y, Sloan SA, Clarke LE, et al. Purification and characterization of progenitor and mature human astrocytes reveals transcriptional and functional differences with mouse. *Neuron*. 2016;89(1):37-53. doi:10.1016/j.neuron.2015.11.013
50. Iwadate Y. Epithelial-mesenchymal transition in glioblastoma progression. *Oncol Lett*. 2016;11(3):1615-1620. doi:10.3892/ol.2016.4113
51. Lau SF, Wu W, Wong HY, et al. The VCAM1-ApoE pathway directs microglial chemotaxis and alleviates Alzheimer's disease pathology. *Nat Aging*. 2023;3(10):1219-1236. doi:10.1038/s43587-023-00491-1
52. Barrera-Ocampo A, Arlt S, Matschke J, et al. Amyloid-beta precursor protein modulates the sorting of testican-1 and contributes to its accumulation in brain tissue and cerebrospinal fluid from patients with Alzheimer disease. *J Neuropathol Exp Neurol*. 2016;75(9):903-916. doi:10.1093/jnen/nlw065
53. King PD, Lubeck BA, Lapinski PE. Nonredundant functions for Ras GTPase-activating proteins in tissue homeostasis. *Sci Signal*. 2013;6(264):re1. doi:10.1126/scisignal.2003669
54. Gelain DP, Dalmolin RJ, Belau VL, Moreira JC, Klamt F, Castro MA. A systematic review of human antioxidant genes. *Front Biosci*. 2009;14(12):4457-4463. doi:10.2741/3541
55. Edgar R, Domrachev M, Lash AE. Gene expression omnibus: NCBI gene expression and hybridization array data repository. *Nucleic Acids Res*. 2002;30(1):207-210. doi:10.1093/nar/30.1.207
56. Feringa FM, van der Kant R. Cholesterol and Alzheimer's disease; from risk genes to pathological effects. *Front Aging Neurosci*. 2021;13:690372. doi:10.3389/fnagi.2021.690372
57. Di Paolo G, Kim TW. Linking lipids to Alzheimer's disease: cholesterol and beyond. *Nat Rev Neurosci*. 2011;12(5):284-296. doi:10.1038/nrn3012
58. Bjorkhem I, Heverin M, Leoni V, Meaney S, Diczfalusy U. Oxysterols and Alzheimer's disease. *Acta Neurol Scand Suppl*. 2006;185:43-49. doi:10.1111/j.1600-0404.2006.00684.x
59. Bjorkhem I, Meaney S. Brain cholesterol: long secret life behind a barrier. *Arterioscler Thromb Vasc Biol*. 2004;24(5):806-815. doi:10.1161/01.ATV.0000120374.59826.1b
60. Andersson M, Elmberger PG, Edlund C, Kristensson K, Dallner G. Rates of cholesterol, ubiquinone, dolichol and dolichyl-P biosynthesis in rat brain slices. *FEBS Lett*. 1990;269(1):15-18. doi:10.1016/0014-5793(90)81107-y
61. Corder EH, Saunders AM, Strittmatter WJ, et al. Gene dose of apolipoprotein E type 4 allele and the risk of Alzheimer's disease in late onset families. *Science*. 1993;261(5123):921-923. doi:10.1126/science.8346443
62. Saunders AM, Strittmatter WJ, Schmechel D, et al. Association of apolipoprotein E allele epsilon 4 with late-onset familial and sporadic

Alzheimer's disease. *Neurology*. 1993;43(8):1467-1472. doi:10.1212/wnl.43.8.1467
63. Nordestgaard LT, Tybjaerg-Hansen A, Nordestgaard BG, Frikke-Schmidt R. Loss-of-function mutation in ABCA1 and risk of Alzheimer's disease and cerebrovascular disease. *Alzheimers Dement*. 2015;11(12):1430-1438. doi:10.1016/j.jalz.2015.04.006
64. Kelly L, Seifi M, Ma R, et al. Identification of intraneuronal amyloid beta oligomers in locus coeruleus neurons of Alzheimer's patients and their potential impact on inhibitory neurotransmitter receptors and neuronal excitability. *Neuropathol Appl Neurobiol*. 2021;47(4):488-505. doi:10.1111/nan.12674
65. Thirumoorthy N, Manisenthil Kumar KT, Shyam Sundar A, Panayappan L, Chatterjee M. Metallothionein: an overview. *World J Gastroenterol*. 2007;13(7):993-996. doi:10.3748/wjg.v13.i7.993
66. Montgomery EB Jr. Heavy metals and the etiology of Parkinson's disease and other movement disorders. *Toxicology*. 1995;97(1-3):3-9. doi:10.1016/0300-483x(94)02962-t
67. Huat TJ, Camats-Perna J, Newcombe EA, Valmas N, Kitazawa M, Medeiros R. Metal toxicity links to Alzheimer's disease and neuroinflammation. *J Mol Biol*. 2019;431(9):1843-1868. doi:10.1016/j.jmb.2019.01.018
68. Pamphlett R, Kum Jew S. Heavy metals in locus ceruleus and motor neurons in motor neuron disease. *Acta Neuropathol Commun*. 2013;1:81. doi:10.1186/2051-5960-1-81
69. Pamphlett R, Mak R, Lee J, et al. Concentrations of toxic metals and essential trace elements vary among individual neurons in the human locus ceruleus. *PLoS One*. 2020;15(5):e0233300. doi:10.1371/journal.pone.0233300
70. de Vries LE, Jongejan A, Monteiro Fortes J, et al. Gene-expression profiling of individuals resilient to Alzheimer's disease reveals higher expression of genes related to metallothionein and mitochondrial processes and no changes in the unfolded protein response. *Acta Neuropathol Commun*. 2024;12(1):68. doi:10.1186/s40478-024-01760-9
71. Ostlund H, Keller E, Hurd YL. Estrogen receptor gene expression in relation to neuropsychiatric disorders. *Ann N Y Acad Sci*. 2003;1007:54-63. doi:10.1196/annals.1286.006
72. Weber LM, Divecha HR, Tran MN, et al. The gene expression landscape of the human locus coeruleus revealed by single-nucleus and spatially-resolved transcriptomics. *Elife*. 2024;12. doi:10.7554/eLife.84628
73. Stubbusch J, Majdazari A, Schmidt M, Schutz G, Deller T, Rohrer H. Generation of the tamoxifen-inducible DBH-Cre transgenic mouse line DBH-CT. *Genesis*. 2011;49(12):935-941. doi:10.1002/dvg.20773
74. Abraira VE, Kuehn ED, Chirila AM, et al. The cellular and synaptic architecture of the mechanosensory dorsal horn. *Cell*. 2017;168(1-2):295-310.e19. doi:10.1016/j.cell.2016.12.010
75. Tao Y, Li X, Dong Q, et al. Generation of locus coeruleus norepinephrine neurons from human pluripotent stem cells. *Nat Biotechnol*. 2024;42:1404-1416. doi:10.1038/s41587-023-01977-4

SUPPORTING INFORMATION

Additional supporting information can be found online in the Supporting Information section at the end of this article.

How to cite this article: Ehrenberg AJ, Sant C, Pereira FL, et al. Pathways underlying selective neuronal vulnerability in Alzheimer's disease: Contrasting the vulnerable locus coeruleus to the resilient substantia nigra. *Alzheimer's Dement*. 2025;21:e70087. https://doi.org/10.1002/alz.70087